ChemPubSoc Europe

DOI: 10.1002/cphc.201800969

CHEMPHYSCHEM Articles

pH Controlled Intersystem Crossing and Singlet Oxygen Generation of 8-Azaadenine in Aqueous Solution

Zhongneng Zhou,[a] Zhubin Hu,[a] Xianwang Zhang,[b] Menghui Jia,[c] Xueli Wang,[a] Hongmei Su,[b] Haitao Sun,[a] Jinquan Chen,*[a, d] and Jianhua Xu[a, d]

Azabases are intriguing DNA and RNA analogues and have been used as effective antiviral and anticancer medicines. However, photosensitivity of these drugs has also been reported. Here, pH-controlled intersystem crossing (ISC) process of 9H 8-azaadenine (8-AA) in aqueous solution is reported. Broadband transient absorption measurements reveal that the hydrogen atom at N9 position can greatly affect ISC of 8-AA and ISC is more favorable when 8-AA is in its neutral form in aqueous solution. The initial excited ππ* (S_2) state evolves through ultrafast internal conversion (IC) (4.2 ps) to the lower-lying nπ* state (S_1), which further stands as a door way state for ISC with a time constant of 160 ps. The triplet state has a lifetime of 6.1 μs. On the other hand, deprotonation at N9 position promotes the IC from the ππ* (S_2) state to the ground state (S_0) and the lifetime of the S_2 state is determined to be 10 ps. The experimental results are further supported by time-dependent density functional theory (TDDFT) calculations. Singlet oxygen generation yield is measured to be 13.8% for the neutral 8-AA while the deprotonated one exhibit much lower yield (<2%), implying that this compound could be a potential pH-sensitized photodynamic therapy agent.

1. Introduction

Nucleobases analogues are the molecules which share similar structure relative to the parent nucleobases, but some of them have distinct biochemical properties such as carcinogenic and antineoplastic effect.[1] Substitution of a carbon atom by a nitrogen atom at certain positions of nucleobases leads to the formation of aza-nucleobases family. These molecules are important due to their potential application as medicine to treat several diseases including cancers.[2] However, phototoxicity potentially leading to DNA damage has been reported in these drugs.[3] Singlet oxygen generation was observed in some azabases in acetonitrile,[4] suggesting they could be potential agents in photodynamic therapy as the case for thionucleobases.[5]

It is reported that singlet oxygen exhibits significant cytotoxicity that is in favor of cancer photodynamic therapy. However, such cytotoxicity can also kill normal cells and its clinical application is limited.[6] In general, physical microenvironment could have great impact on cell's behaviors. For example, cancer cells usually possess extracellular pH (pH_e) as low as 6.3 while normal cells maintain at neutral pH.[7] Such cellular acidosis is generally attributed to the excessive glucose metabolism and poor perfusion.[7–8] Thus, it is expecting that a special light-activated agent can kill the cancer cells while keep the normal ones unharmed.

Singlet oxygen generation in 8-AA acetonitrile solution was observed by Kobayashi et al.[4] However, comprehensive understanding of the excited state deactivation mechanism in 8-AA is still lacking because of existence of multiple potential tautomers of 8-AA in solution.[9] Moreover, the nitrogen atom substitution lowers the p*K*a of 8-AA, leading to significant deprotonation of this molecule at neutral pH.[9c,10] Thus, it is important to identify the tautomers in aqueous solution before further investigation. Contreras et al. theoretically studied the tautomerism of 8-AA in gas phase and aqueous solutions at the MP2/6-31G*//HF/6-31G* level.[9a] They proposed that 9H tautomer of 8-AA is the most stable one in gas phase and found that stability of tautomers in solution is affected by different solvent effect models. Gobbo and coworkers further performed comprehensive calculations on 9H tautomer at the CASPT2//CASSCF level.[9b] Wierzchowski and coworkers reviewed the spectroscopy properties of azaadenine and its derivatives and found that addition of methyl group at N9 position can prevent the formation of 7H and 8H tautomers.[9c,10a] The absorption peak (273 nm), molar extinction coefficient (10500 $M^{-1}cm^{-1}$), fluorescence emission peak (345 nm) of neutral 8-AA are quite close to those of N(9)-methyl-8-AA, implying that 9H tautomer should be the dominant species in aqueous solution at pH = 4.0. Also, such substitution leads N(9)-methyl-8-AA to have only one p*K*a value (2.8) for protonation while 8-AA possesses two p*K*a of 2.7 and 6.3 for protonation and deprotonation, respectively. Such observation further indicates that deprotona-

[a] Z. Zhou, Z. Hu, X. Wang, Prof. H. Sun, Prof. J. Chen, Prof. J. Xu
State Key Laboratory of Precision Spectroscopy
East China Normal University
Shanghai, 200062, China
E-mail: jqchen@lps.ecnu.edu.cn
[b] X. Zhang, H. Su
College of Chemistry
Beijing Normal University
Beijing, 100875, China
[c] Dr. M. Jia
Shanghai Institute of Optics and Fine Mechanics
Shanghai, 201800, China
[d] Prof. J. Chen, Prof. J. Xu
Collaborative Innovation Center of Extreme Optics
Shanxi University
Taiyuan, Shanxi, 030006, China

Supporting information for this article is available on the WWW under https://doi.org/10.1002/cphc.201800969

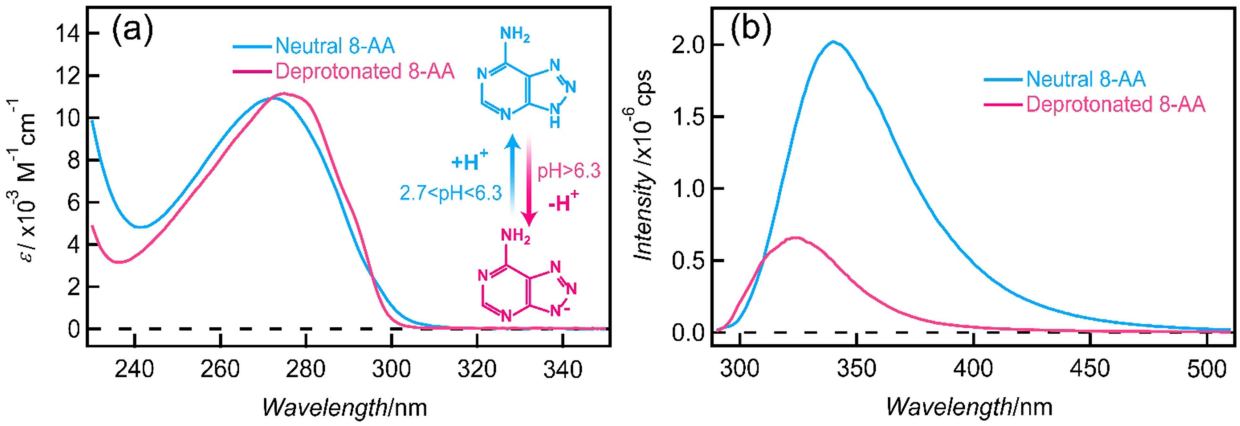

Figure 1. a) Absorption spectra of the neutral and deprotonated form 8-AA. Inset picture represents the acid–base equilibrium. b) The relative emission spectra of neutral and deprotonated 8-AA were measured with the same absorbance at the excitation wavelength (266 nm).

tion most likely happens at N9 position. Based on the previous literature reports and our TDDFT calculations (see detail below), we conclude that 9H tautomer is the dominant species as neutral form of 8-AA and deprotonation is favored at N9 position when pH value is higher than 6.3.

In this work, 9H tautomer of 8-AA in aqueous solution at different pH was studied by steady state absorption and emission spectra, transient absorption spectra, fluorescence up-conversion spectra and the time-dependent density functional theory (TDDFT) calculations. pH controlled intersystem crossing and singlet oxygen generation of 8-AA are reported, suggesting that this compound could be an ideal photodynamic therapy agent targeting only cancer cells which have low pH_e.

2. Results and Discussion

2.1. Steady State Spectra and Theoretical Calculations of 8-AA

Steady state absorption of 8-AA in pH = 4.0 and 10.0 buffer solutions are shown in Figure 1(a). When pH = 4.0, 8-AA is in its neutral form and deprotonated species is presented at pH = 10.0 condition.[9c,11] Both neutral and deprotonated 8-AA exhibit strong absorbance in the UVC region, the absorption maximum is at 272 nm and 276 nm, respectively. These results are quite similar with the canonical nucleobases except for a ~10 nm red-shift.[12] The molar extinction coefficients matched with the data reported by Wierzchowski et al.[10a] Figure 1(b) shows the corresponding emission spectra with the same absorbance at the excitation wavelength (266 nm). Similar to adenine, which is considered to be a non-fluorescence species ($\Phi_{FI} = 2.6 \times 10^{-4}$),[12c,13] 8-AA was reported to have very low fluorescence quantum yield in aqueous solution ($\Phi_{FI} = 8 \times 10^{-3}$).[4] In detail, neutral form 8-AA exhibit emission with the peak located at 340 nm. On the other hand, the emission is apparently quenched and accompanied by a more than 10-nm blue-shift to 324 nm in the deprotonated form 8-AA. Neutral species of 8-AA possesses a 4-fold higher fluorescence quantum yield than that of the deprotonated one. This observation is consistent with the previous reported data.[9c] All the emission were further confirmed to be fluorescence by a deoxygenation experiment (Figure S2). In order to identify the emitting species in 8-AA, the excitation spectra were measured and illustrated in Figure S3. The excitation spectra match well with the absorption spectra for both neutral and deprotonated 8-AA, suggesting that absorption and emission should originate from the same excited state.

Density functional theory (DFT) and time-dependent density functional theory (TDDFT) calculations were performed on 8-AA to reveal the electronic structures and excited-state properties. To further support the observation of 9H tautomer being the major species in the work, we performed the DFT and TDDFT calculations based on 8H and 9H tautomers of 8-AA. (Table S1 and Table S2) The first allowed excited state of 8H tautomer is located at 295 nm which is far from the experiment results. The electrophilicity parameter (ω) of molecule is calculated to reflect the chemical reactivity or stability.[14] Generally, larger electrophilicity parameter means higher chemical reactivity and thus less stability. As shown in Table S2, the ω parameter is calculated to be 2.58 by optimally-tuned LC-BLYP* functional and 3.80 by B3LYP functional for 9H tautomer, and is smaller than that of 8H tautomer (2.79 by LC-BLYP* and 4.24 by B3LYP). The results indicate that the 9H tautomer is more stable than 8H tautomer.

The vertical excitation energies of the lowest singlet- and triplet-excited states involving S_1 to S_4 and T_1 to T_4 are summarized in Table S3. It should be noted that the optimally-tuned density functional method has been proved to provide both qualitative and quantitative predictions of spectral and excited-state properties of organic molecular systems.[15] The representative structures of S_0, S_1, S_2 and T_1 were displayed in Figure S4 and corresponding bond angle and bond length were summarized in Table S4 to S7. The transition details and hole and electron distributions of optimized excited states for neutral and deprotonated 8-AA were shown in Figures S5–S7. The bond length of N7–N8 (1.296 Å) is significantly shortened

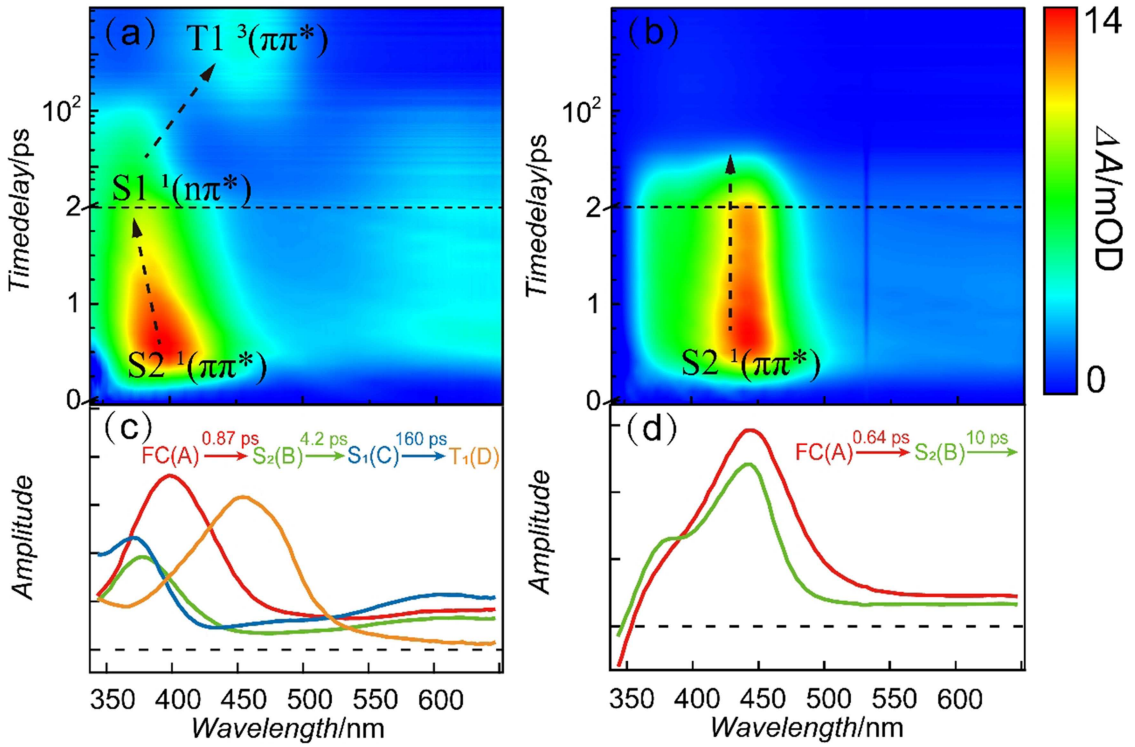

Figure 2. a) and b) 2D broadband transient absorption spectra of 8-AA in pH = 4 and pH = 10 buffer solutions. c) and d) Species associated spectra (SAS) extracted from the global fitting.

with respect to adenine due to the substitution of N on C8.[16] As shown in Table S3, for neutral 8-AA, the first allowed excited state is S_2 ($^1\pi\pi^*$) and the vertical transition energy is found to be 4.48 eV above the ground state. This result is consistent with our steady state absorption spectra. There is also a 4.26 eV S_1 ($^1n\pi^*$) state found in neutral 8-AA. The results are in consistent with previous TDDFT data[4] as well as the results of high level CASPT2//CASSCF calculations.[9b] It is worth to point out that the emission of neutral 8-AA is mainly originated from the S_1 ($^1n\pi^*$) state even though it has small oscillator strength for absorption. The S_1 ($^1n\pi^*$) state energy minimum is calculated adiabatically to be 3.99 eV above the ground state.[9b] The vertical energy difference between S_1 ($^1n\pi^*$) state and S_0 is found to be 3.37 eV, which is identical to our measured emission spectra. Similar behavior of $n\pi^*$ state has also been observed in 9-methylpurine.[17] Therefore, the S_1 ($^1n\pi^*$) state in 8-AA can not be viewed as a "dark" state. On the other hand, our TDDFT results (see Table S3) show that the first allowed excited state of deprotonated 8-AA is also S_2 ($^1\pi\pi^*$) state. The vertical transition energy is 4.49 eV and the oscillation strength is 0.181. Below the S_2 ($^1\pi\pi^*$) state, a S_1 ($^1n\pi^*$) state of 4.34 eV is also presented. In short, the analysis of electronic transitions from TDDFT calculations indicate the similar vertical excitation energies and characters of excited states of deprotonated and neutral 8-AA. This is in good agreement with the very similar measured steady state absorption spectra (Figure 1).

2.2. Broadband Transient Absorption Spectra of 8-AA

To further investigate the excited state properties of 8-AA, femtosecond broad band transient absorption (TA) spectra were measured in different pH buffer solutions (pH = 4.0 and 6.0 for neutral 8-AA; pH = 7.4 and 10.0 for deprotonated 8-AA) and the data were displayed in Figure 2 and Figures S8–S11. For the neutral 8-AA, TA signals (Figures 2a, S8, and S10) arise completely within the initial 500 fs after excitation, exhibiting an excited state absorption (ESA) band centered at 396 nm and a long-tail covering the whole visible region. According to our calculations, the energy of the pump pulse adopted is nearly 0.2 eV higher than the optimized excitation energy, thus we ascribe the initial formed ESA band to absorption of the S_2 ($^1\pi\pi^*$) state. In the following 10 ps, a significant blue-shift is observed with the formation of a new ESA band located at 372 nm, implying the depopulation of the S_2 ($^1\pi\pi^*$) state and the appearance of lower lying S_1 ($^1n\pi^*$) state. In the next 1 ns, the whole spectra gradually decay with another new ESA band grow up at 450 nm. This ESA band exists with no detectable change during the rest of our instrument time window. Kobayashi et al. performed nanosecond transient absorption spectra of 8-AA in acetonitrile.[4] Similar absorption band centered at 450 nm was also observed and attributed to the excited state absorption of triplet state T_1. Also, similar triplet state absorption was observed near 400 nm for purine free base and 9-methylpurine.[17] Additionally, according to Gobbo et al.'s calculations, the intersystem crossing from $^1n\pi^*$ state to $^3\pi\pi^*$

Table 1. Best-fit parameters for broadband transient absorption and up-conversion kinetic traces of neutral and deprotonated 8-AA.

Species	Neutral 8-AA				Deprotonated 8-AA	
	FC region	S_2 ($^1\pi\pi^*$)	S_1 ($^1n\pi^*$)	T_1 ($^3\pi\pi^*$)	FC region	S_2 ($^1\pi\pi^*$)
	τ_1 [ps]	τ_2 [ps]	τ_3 [ps]	τ_4 [μs]	τ_1 [ps]	τ_2 [ps]
broadband TA results	0.87	4.2	160	6.1	0.64	10 ps
Up-converison results	0.90	4.3	130	–	0.87	10.2

state stands as an important pathway for the excited state relaxation due to a large spin orbital coupling (13 cm^{-1}).[9b] Therefore, we also assign the non-decay ESA band to the triplet state T_1 ($^3\pi\pi^*$) state.

Surprisingly, deprotonated 8-AA shows a completely different excited state dynamics when compared with the neutral one. As shown in Figure 2b (also in Figures S9 and S11), in the initial 0.6 ps, only one ESA band at 443 nm appears with a shoulder and it should be originated from the absorption of Frank-Condon (FC) region in the S_2 ($^1\pi\pi^*$) state. Such assignment is common in many nucleobases and their analogues.[18] Only ~2 ps after excitation the TA signals evolve into a broad ESA band with two absorption peaks centered at 440 nm and 380 nm. Next, TA signals decay back to baseline with lifetime of 10 ps.

Representative kinetic traces were selected and illustrated in Figure 3 for a clear comparison. A multi-exponential function was employed to global fit the kinetic traces and fitting

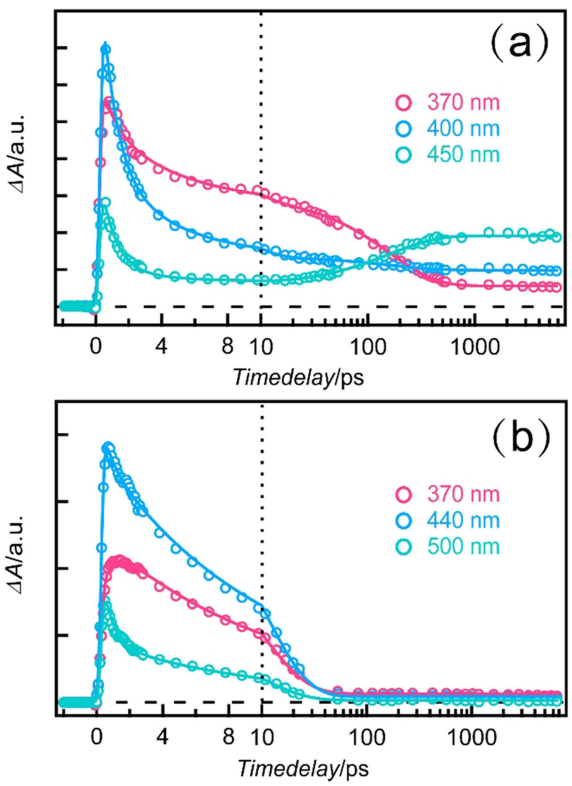

Figure 3. Kinetics of the neutral (a) and deprotonated form of 8-AA (b) for 266 nm excitation. The circles are experimental data and the solid lines represent the best-fits.

parameters are summarized in Table 1. The decay associated spectra (DAS) were illustracted in Figure S12. For neutral 8-AA, three lifetimes were determined to be $\tau_1 = 0.87$ ps, $\tau_2 = 4.2$ ps and $\tau_3 = 160$ ps respectively. We extract species associated spectra (SAS) from global analysis of TA data of netural 8-AA with a sequential kinetic model (Figure 2c). The first SAS (red) shows a broad ESA band which centers at 398 nm. It evolves in 0.87 ps to the 2nd SAS (green) which has the absorption maximum at 380 nm and smaller amplitude. The hundreds of femtosecond efficient depletion from initial excietd $\pi\pi^*$ state has been reported in many canonical nucleobases before.[19] However, in neutral 8-AA's TA spectra, there is a significant blue-shift in the initially formed spectra. Thus, we assign τ_1, the shortest lifetime, to the ultrafast intramolecular vibration relaxation (IVR) from the Frank-Condon region to the energy minimum of the S_2 ($^1\pi\pi^*$) state. The 2nd SAS further blueshifts to the 3rd SAS (blue) which centers at 372 nm with the lifetime of 4.2 ps. Gobbo et al. reported there is a conical intersection (CI) involving S_2 ($^1\pi\pi^*$) state and S_1 ($^1n\pi^*$) state and the energy is 4.24 eV above the ground state.[9b] Such CI was calculated to serve as the converged point on the MEP, implying an efficient depletion of initial populated S_2 ($^1\pi\pi^*$) state. We assign the $\tau_2 =$ 4.2 ps to the lifetime of the S_2 ($^1\pi\pi^*$) state. Next, the 3rd SAS (160 ps lifetime) evolves to the 4th SAS (orange) that exhibits a broad ESA band at 450 nm. Since the 4th SAS has similar band feature with ESA of triplet state, we assign it to the T_1 ($^3\pi\pi^*$) state and its lifetime was determined to be 6.1 μs by the nanosecond time-resolved TA spectra (Figures S13 and S14). As shown in Figure 3(a), at longer delay time (>100 ps), the decay feature at 370 nm is almost identical compared with the signal build-up at 450 nm, indicating that the formation of the triplet state at 450 nm is associated with the depopulation of the species at 370 nm. These data suggest that the 3rd SAS with 160 ps lifetime should be assigned to the S_1 ($^1n\pi^*$) state. Similar time scale intersystem crossing was reported in 9-methylpurine and purine free bases.[17] UV-bleach experiments were conducted and the two lifetimes were determined (Figure S15 and Table S9). Usually, two lifetimes in the bleach signals represent two pathways recover the ground state.[20] In neutral 8-AA, the observed 4.1 ps lifetime should reflect the time takes for S_2 ($^1\pi\pi^*$) state to direct repopulate the ground state as well as vibrational cooling in the hot ground state. The 150 ps lifetime is assigned to S_1 ($^1n\pi^*$) state. An offset with 22% amplitude represents the population on the triplet state which cannot recover to the ground state in our detecting time window. Similar assignment is also obtained by our fluorescence up-conversion data which we will discuss below.

Different from the neutral 8-AA, the efficient depletion of deprotonated 8-AA makes its relaxation mechanism a little bit simpler. Two lifetimes were determined to be $\tau_1 = 0.64$ ps and $\tau_2 = 10$ ps. SAS spectra were extracted and shown in Figure 2(d). For the sub-picosecond τ_1, it is also assigned to the IVR in the S_2 ($^1\pi\pi^*$) state. The τ_2 is attributed to the depopulation of the S_2 ($^1\pi\pi^*$) state which is supported by the blue-shifted SAS spectra in Figure 2(d). UV bleach experiments were also conducted on the deprotonated 8-AA. As illustrated in Figure S15, kinetics of the bleach signal at 275 nm recovers back to baseline very quickly. The lifetime is determined to be 11 ps. Such observation confirms that τ_2 is the lifetime of S_2 ($^1\pi\pi^*$) state in deprotonated 8-AA.

2.3. Femtosecond Time-Resolved Fluorescence Up-Conversion Spectra of 8-AA

In order to further confirm our assignment for the TA spectra, fluorescence up-conversion experiments were performed on neutral and deprotonated 8-AA and the data are displayed in Figure 4. As discussed above, the fluorescence of neutral 8-AA is mainly from the S_1 ($^1n\pi^*$) state and the S_2 ($^1\pi\pi^*$) state may also have some contributions due to its large absorption oscillator strength. As shown in Figure 4(a), the fluorescence kinetics are also fitted by a sequential model for neutral 8-AA. Three time constants were determined to be 0.9 ps, 4.3 ps and 130 ps, respectively (Table 1). These results match with our above TA data. In TA results, there is a 0.87 ps and the similar component was also seen in the up-conversion signal. The 4.3 ps component in up-conversion signal is identical to TA results, which confirms that it is the lifetime of the S_2 ($^1\pi\pi^*$) state.

As for the 130 ps lifetime, it is nearly 30 folds larger than 4.3 ps component, which makes it unlikely to be originated from the S_2 ($^1\pi\pi^*$) state. This component agrees with the lifetime of the S_1 ($^1n\pi^*$) state in TA results under experimental uncertainty and we believe that it should be assigned to the S_1 ($^1n\pi^*$) state. In order to further support our assignment, a solvent-dependent experiment was conducted and the results are shown in Figures S16-17 and Table S8. When dissolved in methanol or ethanol, the emission spectra of 8-AA is broaden and blue-shifted. In ethanol, the up-conversion kinetic traces share the similar feature with those in aqueous solution. The fitting lifetime τ_1 and τ_2 are almost unchanged while the lifetime τ_3 is decreased from 130 ps to 90 ps (Table S8). Such observation suggests that the 130 ps component is responsible for the emission from the S_1 ($^1n\pi^*$) state since lifetime of $n\pi^*$ state is reported to be more sensitive to the solvent environment.[18b]

In deprotonated 8-AA, the emission kinetics show a bi-exponential decay with lifetime of 0.87 ps and 10.2 ps. These lifetimes match the results obtained in the TA experiments, indicating that τ_1 is the IVR process and τ_2 should be the lifetime of the S_2 ($^1\pi\pi^*$) state.

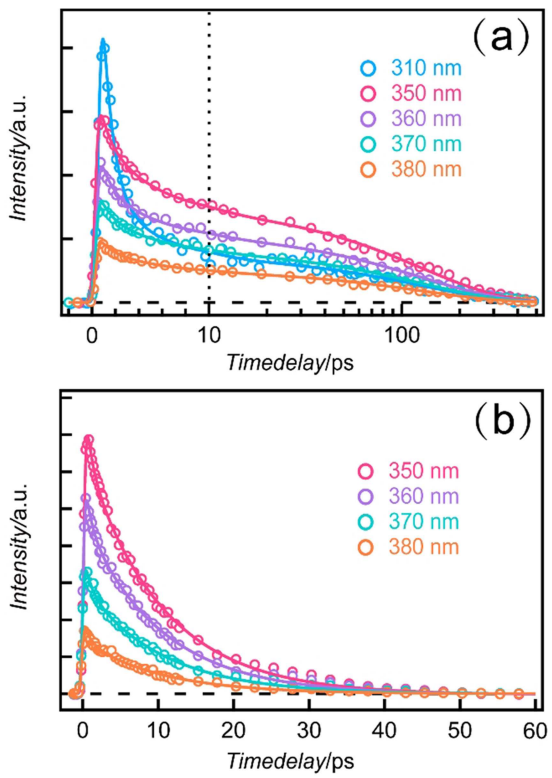

Figure 4. Fluorescence up-conversion data of 8-AA in its a) neutral (pH = 4.0) and b) deprotonated form (pH = 10.0) for 265 nm excitation. The circles are experimental data and the solid lines represent the best-fits.

2.4. Singlet Oxygen Generation of 8-AA

According to the current results, the neutral form 8-AA exhibits a significant triplet state formation yield, whereas the deprotonated form shows a much lower yield. A previous study reveals that triplet state usually stands as a doorway state to generate singlet oxygen.[5b] The pH-controlled triplet state formation yield could lead to pH-controlled singlet oxygen generation. Therefore, time-resolved emission spectra were performed on 8-AA to measure the quantum yield of singlet oxygen generation. The representative emission decay traces were illustrated in Figure 5. Apparently, the neutral 8-AA exhibits one order higher singlet oxygen generation yield (13.8%) than that of the deprotonated 8-AA (~2%). Such pH-controlled singlet oxygen generation was not reported in any aza-nucleobases before.

It is reported that singlet oxygen exhibits significant cytotoxicity which can be used for photodynamic therapy.[6] The traditional use of singlet oxygen's cytotoxicity will also kill the normal cell and its clinical application is limited. However, cancer cells usually have a lower pH_e and this pH value is quite close to the p*K*a of 8-AA. Thus, it is possible that 8-AA could be used to kill cancer cells while keep the normal cells unharmed during photodynamic therapy due to its pH controllable singlet oxygen generation property. To further supporting our hypothesis, transient absorption measurements were also performed on 8-AA in pH = 6.0 and pH = 7.4 buffer solutions. (Figures S10 and S11) The excited state dynamics of 8-AA in pH = 7.4 buffer

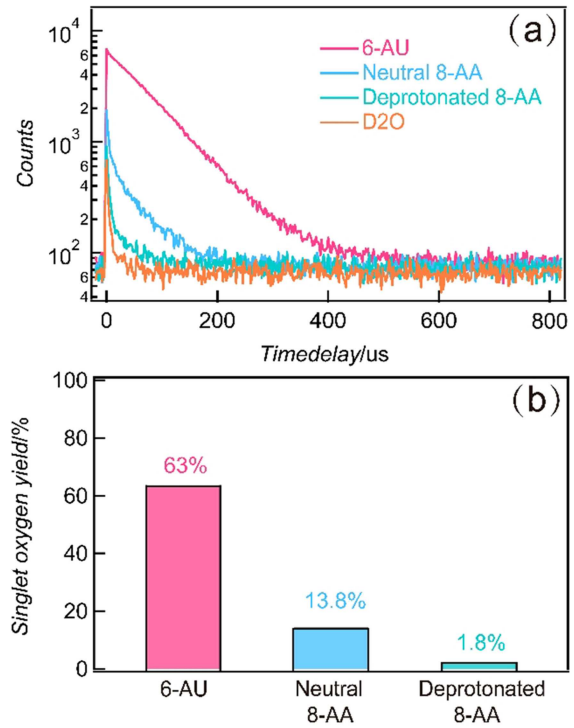

Figure 5. a) Phosphorescence decay traces of singlet oxygen were measured at 1270 nm. b) Singlet oxygen yield of 6-AU, neutral 8-AA, and deprotonated 8-AA, respectively.

(Figure S11) are almost identical compared with the results in pH = 10.0 solutions and internal conversion is the dominant pathway for the excited state relaxation. When 8-AA is in pH = 6.0 buffer solution, the TA signals are a mixture from both neutral and deprotonated form 8-AA. Even though, triplet state is clearly observed in the TA spectra, supporting our hypothesis for the pH controllable singlet oxygen generation. Such behavior suggests that 8-AA could be a potential candidate to be developed as a light-activated agent targeting only cancer cells in photodynamic therapy.

2.5. Proposed Relaxation Mechanism for 8-AA

As an important purine derivative, it should be cautious with the alternative sources to the excited state dynamics. Our TDDFT results shows that the lowest two ππ* states are well separated and the participation of multi bright state (like L_a and L_b state in adenine) cannot occur in 8-AA. Previous theoretical and experimental studies help us to identify that 9H is the only tautomer in aqueous solution.[9b,21] To the best of our knowledge, there is no report about the excited state tautomerization in 8-AA and our results also do not find evidence for excited state tautomer.

It is quite surprising that the hydrogen atom at N9 position have such significant impact on the excited state dynamics of 8-AA. It should be noted that the pH-dependent singlet oxygen generation has also been reported in thio-nucleobase derivatives by Miyata et al.[22] The neutral taDTGuo possesses a higher singlet oxygen yield than the deprotonated one just like the case in 8-AA. The author pointed out that the triplet state lifetime is the main reason for affecting the singlet oxygen generation and similar situation may also exists in 8-AA. It is clear that deprotonation could influence the S_2 ($^1\pi\pi^*$) state relaxation dynamics. For neutral 8-AA, the population on the S_2 ($^1\pi\pi^*$) state could decay to the S_1 ($^1n\pi^*$) state and lead to the formation of triplet state. In deprotonated 8-AA, direct decay from the S_2 ($^1\pi\pi^*$) state to the ground state is dominant. In our TDDFT calculations, we optimized geometries of the S_2 ($^1\pi\pi^*$) state for neutral and deprotonated 8-AA. Deprotonation could lead to the increase of the bond length of N10–C6, C2–N3, C4–C5 and significant decrease of bond angle of N3–C4–C5, N9–C4–C5 in the S_2 ($^1\pi\pi^*$) state. In adenine, the conical intersections of the S_2 ($^1\pi\pi^*$) state to the S_1 ($^1n\pi^*$) state and ground state are characterized by the purine ring torsion and C2 puckering (C2–N3 torsion).[23] Thus, the elongation of C2–N3, C4–C5 and decrease of N3–C4–C5, N9–C4–C5 could also affect the conical intersections on the S_2 ($^1\pi\pi^*$) state, which drives more population directly to the ground state rather than the lower-lying S_1 state and ultimately quenches the triplet state and singlet oxygen generation. As for the S_1 ($^1n\pi^*$) state, the deprotonation on the N9 position increases the bond length of C6–N1, N3–C4, N7–N8, N10–C6 and decreases the bond length of N8–N9. As reported, the C6 puckering and N1-C6 torsion in adenine are responsible for the conical intersection in the $^1n\pi^*$ state.[23a,c] The elongation of C6-N1 bond in 8-AA might also affect the efficiency for intersystem crossing to the triplet state.

Besides that, the spin–orbit coupling (SOC) between S_1 and T_1 calculated using Dalton2016 at B3LYP/aug-cc-pVTZ and CAM-B3LYP/aug-cc-pVTZ level were computed to be about 7.24 cm^{-1} and 6.54 cm^{-1} respectively. These are on the same magnitude of 13.4 cm^{-1} calculated at the CASPT2//CASSCF level,[9b] indicating a fast intersystem crossing from S_1 to the T_1 state; The smaller SOC value of 2.50 cm^{-1} and 2.72 cm^{-1} between S_1 ($^1n\pi^*$) state and T_1 ($^3\pi\pi^*$) state in the deprotonated form (Table S11) suggests a weaker spin-orbit coupling that further hinder the intersystem crossing process. The long-living residual TA signal at ~350–500 nm is likely to be the tiny triplet state absorption of the deprotonated form, which further cause to the 1.8% formation of singlet oxygen. In general, the smaller spin–orbit coupling might also be the reason why triplet state quenched in deprotonated 8-AA.

Additionally, excited state dynamics affected by the deprotonation was also found in hypoxanthine. Neutral hypoxanthine exhibits only an ultrafast decay (< 0.2 ps) while deprotonated hypoxanthine shows another much longer decay (19 ps).[24] It was suggested that the deprotonation on the N9 position may have a long-range effect in changing the planarity of pyrimidine ring and the C2 puckering, which will finally lead to the differences on the emissive state surface and the accessibility to the conical intersection. Similar phenomena could also happen in 8-AA.

Based on our current results, the comprehensive relaxation mechanisms of neutral and deprotonated 8-AA are summarized in Scheme 1. For the neutral one, the initial populated S_2 ($^1\pi\pi^*$)

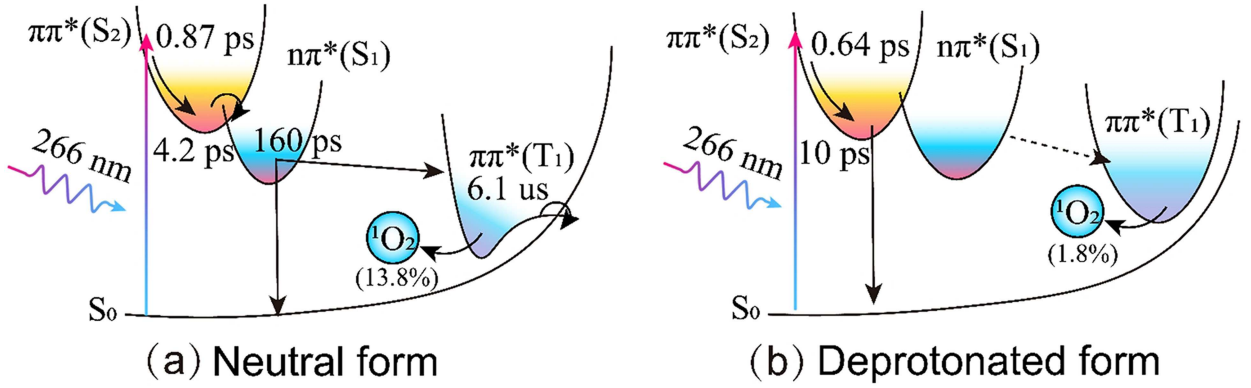

Scheme 1. Proposed main relaxation mechanism for the neutral and deprotonated form 8-AA.

state can evolve to the minimum of S_2 ($^1\pi\pi^*$) state with lifetime of 0.87 ps. Then S_2 ($^1\pi\pi^*$) state can further decay to the S_1 ($^1n\pi^*$) state or directly repopulate the ground state with a lifetime of 4.2 ps. After that, the population on the S_1 ($^1n\pi^*$) state can intersystem cross to T_1 ($^3\pi\pi^*$) state and the time constant is 160 ps. Singlet oxygen generation quantum yield is found to be 13.8%. The triplet state T_1 ($^3\pi\pi^*$) itself has a lifetime of 6.1 μs in aqueous solution (details in supporting information). On the other hand, in the deprotonated 8-AA, the initial populated S_2 ($^1\pi\pi^*$) state can decay to the minimum of S_2 ($^1\pi\pi^*$) state with 0.64 ps lifetime. Then, almost all the population in the S_2 ($^1\pi\pi^*$) state return back to the ground state with lifetime of 10 ps. Only few singlet oxygen is detected in deprotonated 8-AA aqueous solution due to its tiny generation yield (1.8%).

3. Conclusions

Excited-state dynamics of 8-AA in aqueous solutions have been comprehensively studied by broad band femtosecond transient absorption spectra. pH controlled intersystem crossing and singlet oxygen generation were discovered. Two different relaxation mechanisms have been proposed for neutral and deprotonated form 8-AA. Neutral form 8-AA exhibits the significant triplet state yield and moderate singlet oxygen generation yield. Deprotonation at N9 position makes the depletion from the ππ* state more favorable than the neutral one. Such efficient depletion dominates the relaxation of deprotonated 8-AA and barely triplet state can be accessed. The pH-controlled singlet oxygen generation increases the possibility for potential biological and clinical application. Overall, these results show that the photophysical and photochemical properties of azabases are greatly dependent on their structures. It is our hope that this work will stimulate more future investigations on the excited state dynamics of the nitrogen substituted nucleic acids and utilize their unique photochemical properties to design new light-activated agent for photodynamic therapy.

Experimental Section

Chemicals

8-azaadenine is purchased from J&K Chemical Ltd. (Shanghai, China) and used as received without further purification. Two different pH value (pH = 4.0 ± 0.2 and pH = 10.0 ± 0.2) buffer solutions are adopted to keep chemical conformation of the sample in neutral and deprotonated form. In detail, the pH = 4.0 buffer was prepared with a mixture of sodium dihydrogen phosphate (0.2 M) and citric acid (0.1 M). The pH = 10 buffer was prepared with a mixture of sodium carbonated (0.1 M) and sodium bicarbonate (0.1 M). The pH = 6.0 and pH = 7.4 solutions are PBS buffer solutions. Water used in the experiment is deionized water with 18.2 MΩ·cm resistivity (Direct-Q3 UV, Merck Millipore).

Steady-State Absorption and Emission Spectra

The steady state UV-vis absorption spectra and emission spectra were measured by a double beam UV-vis spectrometer (TU1901, Beijing Purkinje General Instrument Co. Ltd.) and steady state fluorescence spectrometer (FluoroMax-4, Horiba, Jobin Yvon) respectively. All spectra were performed using a 2 mm quartz cuvette. Molar extinction coefficients of 8-AA were measured according to Lambert-Beer's law. For emission spectra, the excitation wavelength is 266 nm. All experiments were carried out at the room temperature.

Femtosecond Broadband Transient Absorption and Fluorescence Up-Conversion Spectroscopy

Excited-state dynamics of 8-AA were investigated using broadband femtosecond transient absorption spectroscopy. The experiment setup has been reported in the previous investigation.[18a] Briefly, a Ti:sapphire amplifier (Astrella, Coherent Inc.) generates a fundamental beam with the power output of 7 W. Almost 500 mW of the fundamental beam is adopted to generate a deep UV 266 nm pulse by third harmonic generation. The broadband transient absorption spectra were obtained by the commercial spectrometer (Helios fire, Ultrafast System). The polarization between the pump and probe beams was set to be magic angle (54.7°). During the experiments, the sample were stored in a 2 mm quartz cell and continuously stirred by a stir bar to avoid degradation.

The femtosecond time-resolved fluorescence spectra were collected by a home-built fluorescence up-conversion setup which have

been reported before.[25] In brief, the pump pulse is generated by an optical parametric amplifier (OPerA Solo, Coherent Inc.) and purified by a pair of UV prisms. The gate pulse is a small portion of 800 nm fundamental beam. The sample is held in a continuously spinning UV quartz disk to avoid photodamage. The fluorescence is collected by a pair of parabolic focus mirrors and then focused into a 0.2 mm BBO crystal to sum frequency with the 800 nm gate pulse. The up-conversion signals are sent to a monochromator (Omni-k500, Zolix), and detected by a photomultiplier tube (CR317, Hamamatsu). The signals are recorded by a home-made software written using LabWindows.

Time-Dependent Density Functional Theory Calculations

In order to interpret the experimental results, density functional theory (DFT) and time-dependent density functional theory (TDDFT) calculations were performed using GAUSSIAN09 software.[26] The ground-state geometries are initially optimized at the B3LYP/6-311++G** level. The vertical excitation energies of the lowest singlet- and triplet-excited states involving S_1 to S_4 and T_1 to T_4 for neutral and deprotonated 8-AA are calculated using optimally-tuned LC-BLYP* functional ($\omega = 0.134$ bohr^{-1}) with the 6-311++G** basis set (see Table S1). The polarizable continuum model (PCM) was employed to take into account the effects of the dielectric medium of water. The geometries of the S_1 to S_4 and T_1 to T_4 states are optimized using the implemented TDDFT gradients at the PCM (water)-LC-BLYP*/6-311++G** level. To test the reliability of DFT method employed in this work, three different density functionals including LC-BLYP, CAM-B3LYP and B3LYP were performed for comparison. In general, the optimally-tuned LC-BLYP* functional method employed in this work reproduces the experimental data very well and performs best among different DFT methods.

The Spin-orbit coupling (SOC) between singlet and triplet states of neutral and deprotonated 8-AA were further evaluated by Dalton2016 program,[27] using the Breit–Pauli operator with atomic mean field (AMF) approximation,[28] with the previously B3LYP/6-311++G** optimized geometries being calculated at the (CAM)-B3LYP/aug-cc-pVTZ level. Since the density functionals available in Dalton2016 is limited, only B3LYP and CAM-B3LYP have been employed for SOC calculation and they are found to produce similar SOC values.

Acknowledgements

This study was funded by National Nature Science Foundation of China (No. 11674101 and 21873030 to J.C.; No. 21425313 to H.S.; No. 21603074 to H.S.). H.S. also thanks the funding of "Chenguang Program" by Shanghai Education Development Foundation and Shanghai Municipal Education Commission (16CG25).

Conflict of Interest

The authors declare no conflict of interest.

Keywords: 8-azaadenine · intersystem crossing · pH · singlet oxygen · transient absorption

[1] a) A. Massey, Y. Z. Xu, P. Karran, *Curr. Biol.* **2001**, *11*, 1142–1146; b) X. Zhang, G. Jeffs, X. Ren, P. O'Donovan, B. Montaner, C. M. Perrett, P. Karran, Y.-Z. Xu, *DNA Repair* **2007**, *6*, 344–354; c) S. W. Pridgeon, R. Heer, G. A. Taylor, D. R. Newell, K. O'Toole, M. Robinson, Y. Z. Xu, P. Karran, A. V. Boddy, *Br. J. Cancer* **2011**, *104*, 1869–1876; d) K. Raška, M. Jurovčík, Z. Šormová, F. Šorm, *Collect. Czech. Chem. Commun.* **1965**, *30*, 3001–3006.

[2] a) J. A. Montgomery, *Cancer Res.* **1959**, *19*, 447–463; b) B. J. Broughton, P. Chaplen, P. Knowles, E. Lunt, D. L. Pain, K. R. Wooldridge, R. Ford, S. Marshall, J. L. Walker, D. R. Maxwell, *Nature* **1974**, *251*, 650–652; c) E. N. Spremulli, G. W. Crabtree, D. L. Dexter, C. Shih Hsi, D. M. Farineau, L. Y. Ghoda, D. L. McGowan, I. Diamond, R. E. Parks, P. Calabresi, *Biochem. Pharmacol.* **1982**, *31*, 2415–2421.

[3] a) M. S. Chen, P. K. Chang, W. H. Prusoff, *J. Biol. Chem.* **1976**, *251*, 6555–6561; b) P. O'Donovan, C. M. Perrett, X. Zhang, B. Montaner, Y.-Z. Xu, C. A. Harwood, J. M. McGregor, S. L. Walker, F. Hanaoka, P. Karran, *Science* **2005**, *309*, 1871–1874.

[4] T. Kobayashi, H. Kuramochi, Y. Harada, T. Suzuki, T. Ichimura, *J. Phys. Chem. A* **2009**, *113*, 12088–12093.

[5] a) Y. Harada, T. Suzuki, T. Ichimura, Y.-Z. Xu, *J. Phys. Chem. B* **2007**, *111*, 5518–5524; b) M. Pollum, S. Jockusch, C. E. Crespo-Hernández, *J. Am. Chem. Soc.* **2014**, *136*, 17930–17933; c) S. Mai, M. Pollum, L. Martínez-Fernández, N. Dunn, P. Marquetand, I. Corral, C. E. Crespo-Hernández, L. González, *Nat. Commun.* **2016**, *7*, 13077; d) M. Pollum, M. Lam, S. Jockusch, C. E. Crespohernández, *ChemMedChem* **2018**, *13*, 1–8.

[6] a) M. C. DeRosa, R. J. Crutchley, *Coord. Chem. Rev.* **2002**, *233*, 351–371; b) K. R. Weishaupt, C. J. Gomer, T. J. Dougherty, *Cancer Res.* **1976**, *36*, 2326–2329.

[7] a) R. J. Gillies, N. Raghunand, M. L. Garciamartin, R. A. Gatenby, *IEEE Eng. Med. Biol.* **2004**, *23*, 57; b) I. F. Tannock, D. Rotin, *Cancer Res.* **1989**, *49*, 4373–4384.

[8] N. R. Jagannathan, Z. M. Bhujwalla, *NMR Biomed.* **2011**, *24*, 582–591.

[9] a) J. G. Contreras, S. T. Madariaga, J. B. Alderete, *J. Phys. Org. Chem.* **1998**, *11*, 392–396; b) J. P. Gobbo, A. C. Borin, *J. Phys. Chem. B* **2012**, *116*, 14000–14007; c) J. Wierzchowski, J. M. Antosiewicz, D. Shugar, *Mol. BioSyst.* **2014**, *10*, 2756–2774.

[10] a) J. Wierzchowski, B. Wielgus-Kutrowska, D. Shugar, *Biochim. Biophys. Acta Gen. Subj.* **1996**, *1290*, 9–17; b) M. Pollum, S. Jockusch, C. E. Crespo-Hernández, *Phys. Chem. Chem. Phys.* **2015**, *17*, 27851–27861.

[11] K. Takazawa, *J. Chem. Soc. C* **1968**, *30*, 344–347.

[12] a) C. E. Crespo-Hernández, B. Cohen, P. M. Hare, B. Kohler, *Chem. Rev.* **2004**, *104*, 1977–2019; b) C. T. Middleton, K. de La Harpe, C. Su, Y. K. Law, C. E. Crespo-Hernández, B. Kohler, *Annu. Rev. Phys. Chem.* **2009**, *60*, 217–239; c) M. Pollum, L. Martinez-Fernandez, C. E. Crespo-Hernández, in *Photoinduced Phenomena in Nucleic Acids I: Nucleobases in the Gas Phase and in Solvents, Vol. 355* (Eds.: M. Barbatti, A. C. Borin, S. Ullrich), Springer, **2015**, pp. 245–327.

[13] P. R. Callis, *Ann. Rev. Phys. Chem.* **1983**, *34*, 329–357.

[14] a) R. G. Parr, L. v. Szentpály, S. Liu, *J. Am. Chem. Soc.* **1999**, *121*, 1922–1924; b) L. von Szentpály, *J. Phys. Chem. A* **1998**, *102*, 10912–10915; c) Z. Bin, H. Zhubin, J. Yanrong, H. Xiao, S. Zhenrong, S. Haitao, *J. Phys. Condens. Matter* **2018**, *30*, 215501.

[15] a) H. Sun, C. Zhong, J.-L. Brédas, *J. Chem. Theory Comput.* **2015**, *11*, 3851–3858; b) H. Sun, S. Zhang, C. Zhong, Z. Sun, *J. Comput. Chem.* **2016**, *37*, 684–693; c) X. Tian, H. Sun, Q. Zhang, C. Adachi, *Chin. Chem. Lett.* **2016**, *27*, 1445–1452.

[16] L. Serrano-Andrés, M. Merchán, A. C. Borin, *Proc. Natl. Acad. Sci. USA* **2006**, *103*, 8691–8696.

[17] C. E. Crespo-Hernández, L. Martínez-Fernández, C. Rauer, C. Reichardt, S. Mai, M. Pollum, P. Marquetand, L. González, I. s. Corral, *J. Am. Chem. Soc.* **2015**, *137*, 4368–4381.

[18] a) X. Wang, Z. Zhou, Y. Tang, J. Chen, D. Zhong, X. Jianhua, *J. Phys. Chem. B* **2018**, *122*, 7027–7037; b) C. Ma, C. C. Cheng, C. T. Chan, R. C. Chan, W. M. Kwok, *Phys. Chem. Chem. Phys.* **2015**, *17*, 19045–19057; c) N. K. Schwalb, F. Temps, *J. Phys. Chem. A* **2009**, *113*, 13113–13123.

[19] a) V. I. Prokhorenko, A. Picchiotti, M. Pola, A. G. Dijkstra, R. J. D. Miller, *J. Phys. Chem. Lett.* **2016**, *7*, 4445–4450; b) J. M. L. Pecourt, J. Peon, B. Kohler, *J. Am. Chem. Soc.* **2000**, *123*, 9348–9349.

[20] P. M. Hare, C. E. Crespo-Hernández, B. Kohler, *Proc. Natl. Acad. Sci. USA* **2007**, *104*, 435–440.

[21] J. Wierzchowski, *Nucleosides Nucleotides Nucleic* **2014**, *33*, 626–644.

[22] S. Miyata, M. Hoshino, T. Isozaki, T. Yamada, H. Sugimura, Y.-Z. Xu, T. Suzuki, *J. Phys. Chem. B* **2018**, *122*, 2912–2921.

[23] a) E. Fabiano, W. Thiel, *J. Phys. Chem. A* **2008**, *112*, 6859–6863; b) M. Barbatti, H. Lischka, *J. Am. Chem. Soc.* **2008**, *130*, 6831–6839; c) Y. Lei, S. Yuan, Y. Dou, Y. Wang, Z. Wen, *J. Phys. Chem. A* **2008**, *112*, 8497–8504.

[24] J. P. Villabona-Monsalve, R. Noria, S. Matsika, J. Peon, *J. Am. Chem. Soc.* **2012**, *134*, 7820–7829.
[25] M. H. Jia, H. Yi, M. F. Chang, X. D. Cao, L. Li, Z. N. Zhou, H. F. Pan, Y. Chen, S. J. Zhang, J. H. Xu, *J. Photochem. Photobiol. B* **2015**, *149*, 243–248.
[26] a) M. J. Frisch, G. W. Trucks, H. B. Schlegel, G. E. Scuseria, M. A. Robb, J. R. Cheeseman, G. Scalmani, V. Barone, B. Mennucci, G. A. Petersson, H. Nakatsuji, M. Caricato, X. Li, H. P. Hratchian, A. F. Izmaylov, J. Bloino, G. Zheng, J. L. Sonnenberg, M. Hada, M. Ehara, K. Toyota, R. Fukuda, J. Hasegawa, M. Ishida, T. Nakajima, Y. Honda, O. Kitao, H. Nakai, T. Vreven, J. Montgomery, J. A., J. E. Peralta, F. Ogliaro, M. Bearpark, J. J. Heyd, E. Brothers, K. N. Kudin, V. N. Staroverov, R. Kobayashi, J. Normand, K. Raghavachari, A. Rendell, J. C. Burant, S. S. Iyengar, J. Tomasi, M. Cossi, N. Rega, N. J. Millam, M. Klene, J. E. Knox, J. B. Cross, V. Bakken, C. Adamo, J. Jaramillo, R. Gomperts, R. E. Stratmann, O. Yazyev, A. J. Austin, R. Cammi, C. Pomelli, J. W. Ochterski, R. L. Martin, K. Morokuma, V. G. Zakrzewski, G. A. Voth, P. Salvador, J. J. Dannenberg, S. Dapprich, A. D. Daniels, Ö. Farkas, J. B. Foresman, J. V. Ortiz, J. Cioslowski, D. J. Fox, *Vol. D.01*, Gaussian Inc., Wallingford CT, **2009**; b) M. E. Casida, C. Jamorski, K. C. Casida, D. R. Salahub, *J. Chem. Phys.* **1998**, *108*, 4439–4449.
[27] K. Aidas, C. Angeli, K. L. Bak, V. Bakken, R. Bast, L. Boman, O. Christiansen, R. Cimiraglia, S. Coriani, P. Dahle, E. K. Dalskov, U. Ekström, T. Enevoldsen, J. J. Eriksen, P. Ettenhuber, B. Fernández, L. Ferrighi, H. Fliegl, L. Frediani, K. Hald, A. Halkier, C. Hättig, H. Heiberg, T. Helgaker, A. C. Hennum, H. Hettema, E. Hjertenæs, S. Høst, I.-M. Høyvik, M. F. Iozzi, B. Jansík, H. J. A. Jensen, D. Jonsson, P. Jørgensen, J. Kauczor, S. Kirpekar, T. Kjærgaard, W. Klopper, S. Knecht, R. Kobayashi, H. Koch, J. Kongsted, A. Krapp, K. Kristensen, A. Ligabue, O. B. Lutnæs, J. I. Melo, K. V. Mikkelsen, R. H. Myhre, C. Neiss, C. B. Nielsen, P. Norman, J. Olsen, J. M. H. Olsen, A. Osted, M. J. Packer, F. Pawlowski, T. B. Pedersen, P. F. Provasi, S. Reine, Z. Rinkevicius, T. A. Ruden, K. Ruud, V. V. Rybkin, P. Sałek, C. C. M. Samson, A. S. de Merás, T. Saue, S. P. A. Sauer, B. Schimmelpfennig, K. Sneskov, A. H. Steindal, K. O. Sylvester-Hvid, P. R. Taylor, A. M. Teale, E. I. Tellgren, D. P. Tew, A. J. Thorvaldsen, L. Thøgersen, O. Vahtras, M. A. Watson, D. J. D. Wilson, M. Ziolkowski, H. Ågren, *WIREs Comput. Mol. Sci.* **2014**, *4*, 269–284.
[28] a) A. D. Becke, *Phys. Rev. A* **1988**, *38*, 3098–3100; b) A. D. Becke, *J. Chem. Phys.* **1993**, *98*, 5648–5652.

Manuscript received: October 16, 2018
Revised manuscript received: January 30, 2019
Accepted manuscript online: January 31, 2019
Version of record online: February 15, 2019